A Journal of the Gesellschaft Deutscher Chemiker

Angewandte International Edition GDCh Chemie

www.angewandte.org

## Accepted Article

**Title:** Dual-ion intercalation and high volumetric capacitance in a two-dimensional non-porous coordination polymer

**Authors:** Harish Banda, Jin-Hu Dou, Tianyang Chen, Yugang Zhang, and Mircea Dincă



**To be cited as:** *Angew. Chem. Int. Ed.* 10.1002/anie.202112811

**Link to VoR:** https://doi.org/10.1002/anie.202112811

WILEY-VCH

10.1002/anie.202112811

WILEY-VCH

RESEARCH ARTICLE

# Dual-ion intercalation and high volumetric capacitance in a two-dimensional non-porous coordination polymer

Harish Banda[⊥][a], Jin-Hu Dou[⊥][a], Tianyang Chen[a], Yugang Zhang[b] and Mircea Dincă*[a]

[a] Dr. H. Banda, Dr. J-H. Dou, T. Chen, Prof. M. Dincă
Department of Chemistry
Massachusetts Institute of Technology
77 Massachusetts Avenue, Cambridge, MA 02139 (USA)
E-mail: mdinca@mit.edu
[b] Dr. Y. Zhang
Center for Functional Nanomaterials
Brookhaven National Laboratories
735 Brookhaven Avenue, Upton, NY 11973 (USA)
⊥ These authors contributed equally

Supporting information for this article is given via a link at the end of the document.

**Abstract:** Intercalation is a promising ion sorption mechanism for enhancing the energy density of electrochemical capacitors (ECs) because it offers enhanced access to electrochemical surface area. It requires rapid transport of ions in and out of a host material and it must occur without phase transformation. Materials that fulfil these requirements are rare; those that do, intercalate almost exclusively cations. Herein, we show that $Ni_3$(benzenehexathiol) ($Ni_3$BHT), a non-porous two-dimensional (2D) layered coordination polymer (CP), intercalates both cations and anions with a variety of charges. Whereas cation intercalation is pseudocapacitive, anions intercalate in a purely capacitive fashion. The excellent EC performance of $Ni_3$BHT provides a general basis for investigating similar dual-ion intercalation mechanisms in the large family of non-porous 2D CPs.

## Introduction

Electrochemical capacitors (ECs) store energy through reversible ion sorption at the electrode-electrolyte interface. They have emerged as reliable, high-power, and low-energy storage devices that complement rechargeable batteries.[1,2] Typically, ion sorption at the interface is studied as a surface-based process, wherein the total energy stored in an EC is determined by the available electrode surface area, also known as the electrochemical surface area. A major strategy toward enhancing energy densities of ECs has been to increase the specific surface area (SSA), in the hope that it would correlate with greater availability of surface sites for ion sorption.[3,4] However, the SSA is not equivalent with the electrochemical surface area, and increasing bulk porosity does not necessarily give rise to increased capacitance.[3] A more directed strategy to increase charge storage is the use of intercalation, an ion sorption pathway that involves reversible insertion of ionic species into the bulk of a layered electrode material. Although widely used in battery chemistries, intercalation has generally been considered too slow for usage in high-power devices such as ECs.[5–8] Nevertheless, research over the past decade has identified select-few inorganic materials, such as $Nb_2O_5$, $MoS_2$, $LaMnO_3$ and $Ti_3C_2$ (MXenes), that exhibit a non-traditional intercalation behavior with capacitor-like electrochemical signatures, such as fast charge delivery over a time scale of minutes.[9–18] Importantly, these materials exhibit

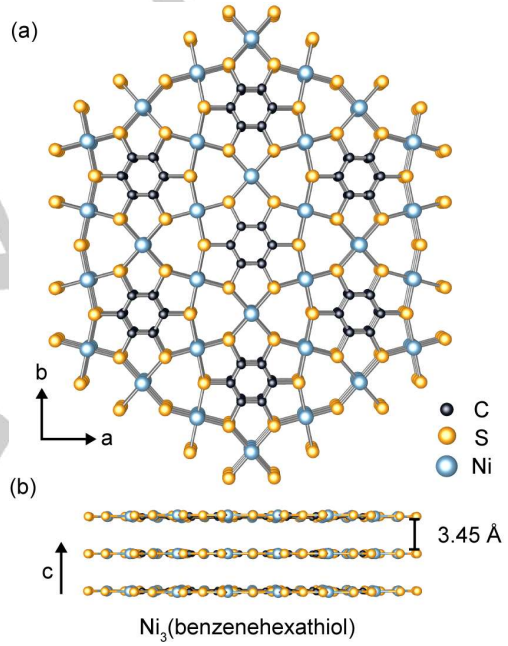


***Figure 1.*** Simulated structure of $Ni_3$BHT viewed along the (a) *c*-direction and parallel to the *ab* plane.

multi-fold increments in energy densities over conventional electric double-layer capacitors (EDLCs), whilst maintaining comparable power densities.

The precise origin of enhanced energy density is still debated, with some proposing that faradaic sites within the bulk contribute to charge storage,[5,19,20] and that electrolyte charges rapidly reach these sites via two-dimensional (2D) tunnels/channels.[21–23] This behavior is distinguished from its conventional battery counterpart and is termed intercalation-pseudocapacitance.[4,9] Other reports backed by modelling approaches dispute the concept of pseudocapacitance and instead explain the capacitive features in non-porous electrodes by treating the materials as electronic conductors that undergo ion sorption at the large surface area made available as a result of intercalation.[24,25]

10.1002/anie.202112811




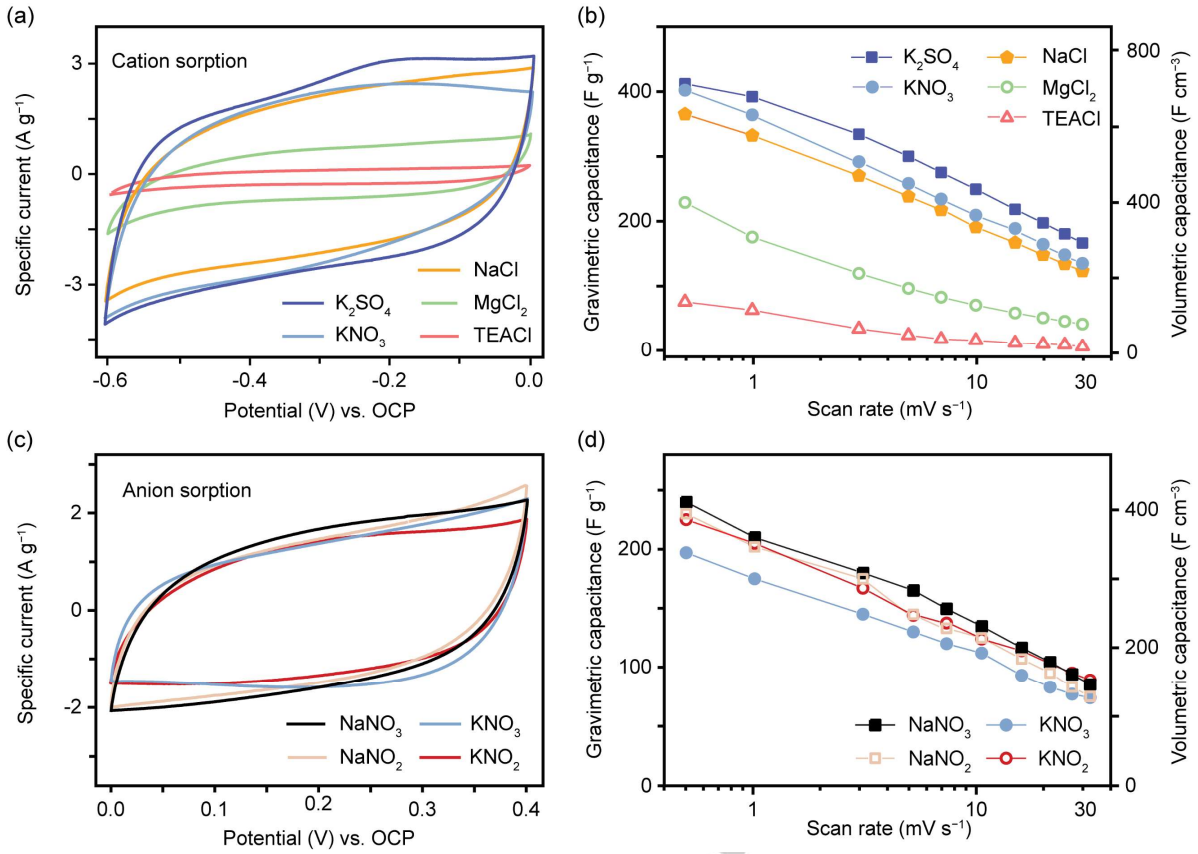


***Figure 2.*** Cyclic voltammograms (CVs) of $Ni_3BHT$ in several 0.5 M aqueous electrolytes under (a) negative and (c) positive polarization vs. open circuit potentials (OCP) at a scan rate of 10 mV $s^{-1}$. Gravimetric and volumetric power capabilities of $Ni_3BHT$ under (b) negative and (d) positive polarization calculated from CVs recorded at scan rates ranging from 0.5 to 30 mV $s^{-1}$. The scan rates chosen here correspond to variable discharge times ranging from 20 min and 20 s.

This ongoing discussion notwithstanding, both descriptions make it clear that intercalation electrodes for EC must have good electronic conduction, swift ion-transport pathways, and weak (if any) energy interactions with the electrolyte components. The emerging class of 2D coordination polymers (CPs) meet these difficult criteria, and additionally offer tremendous compositional diversity by accommodating abundant metal ions and organic linkers in π-d conjugated 2D layers.[26–33] The distinction between non-porous CPs and porous CPs, also known as MOFs, is important here: the latter have seen greater interest in the context of ECs because they naturally exhibit higher SSA,[34–38] while non-porous CPs have largely been overlooked in this sense. Here, we show that $Ni_3$(benzenehexathiol) ($Ni_3BHT$), a non-porous two-2D CP that was recently shown to intercalate $Li^+$,[39] reversibly intercalates not just cations, but also anions, thereby qualifying as a rare dual-ion intercalation electrode material. Detailed electrochemical studies reveal a unique intercalation behavior in $Ni_3BHT$ that involves charge-transfer events, often referred to as pseudocapacitive, under cathodic potentials, and purely capacitive behavior under anodic bias.

## Results and Discussion

We previously reported the synthesis of $Ni_3BHT$, wherein $Ni^{2+}$ ions and BHT linkers are arranged in a densely-packed 2D structure with an inter-layer spacing of 3.45 Å (Figure 1) and SSA of 25 $m^2$ $g^{-1}$.[39] The sulfur atoms on the BHT moieties each coordinate with two $Ni^{2+}$ ions in square-planar fashion to yield an extended π-d conjugated framework with high electrical conductivity of 5 S $cm^{-1}$, sufficient for a potential use in ECs. Having highlighted the intriguing ability of $Ni_3$(BHT) to intercalate Li ions, we sought to explore its interaction with other mono and multi-atomic ions spanning both reductive and oxidative polarizations. Aqueous solutions of several inorganic and organic chlorides, sulfates, and nitrates were used as the electrolytes for this study. Tests were performed in a three-electrode cell configuration and the applied potentials are reported with respect to the open circuit potentials (OCP). This representation with OCP denotes the applied bias as either positive or negative with respective to the steady-state potential, allowing for a direct comparison of cation (or anion) sorption in different electrolytes. Nevertheless, potentials are also given with respect to Ag/AgCl for comparison purposes.

10.1002/anie.202112811




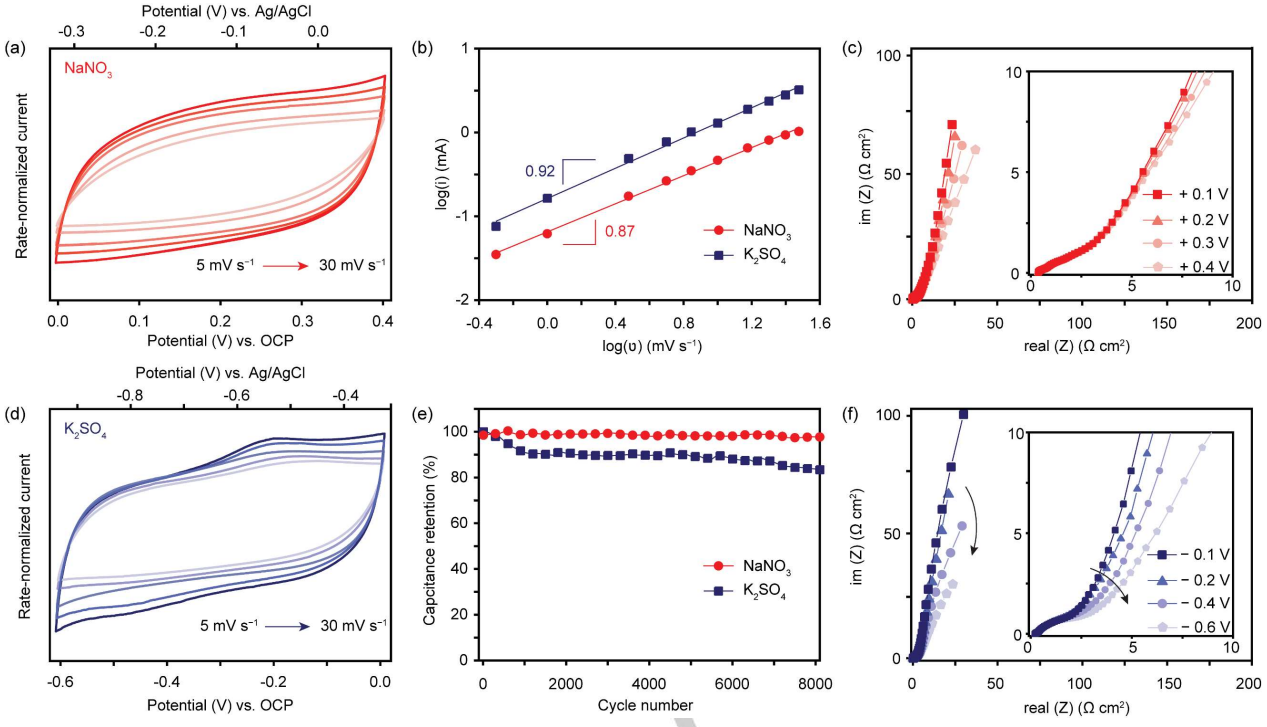


***Figure 3.*** CVs of $Ni_3BHT$ obtained in (a) 0.5 M $NaNO_3$ under positive polarization of 0 to 0.4 V vs. OCP and in (d) 0.5 M $K_2SO_4$ under negative polarization of 0 to -0.6 V vs. OCP at scan rates ranging from 5 to 30 mV $s^{-1}$. (b) Peak current vs. scan rate analysis preformed at polarizations of 0.2 V and -0.2 V vs. OCP in $NaNO_3$ and $K_2SO_4$ electrolytes, respectively. Data were fit and the slope of the curve is calculated to extrapolate *b* value using Equation 1. Nyquist plots of $Ni_3BHT$ in (c) $NaNO_3$ and (f) $K_2SO_4$ electrolytes at various positive and negative potentials, respectively. (d) Cycling performance of $Ni_3BHT$ in both the electrolytes over 8000 cycles at a scan rate of 30 mV $s^{-1}$.

**Dual-ion intercalation:** A steady-state cyclic voltammogram (CV) of a $Ni_3BHT$ electrode prepared on Ni foam in 0.5 M $K_2SO_4$ displays a quasi-rectangular shape under negative polarization (Figure 2a), indicating capacitive sorption of $K^+$ ions throughout a stable potential window of 0 to -0.6 V vs. OCP (Figure S1). Similar CVs are observed in other alkali metal electrolytes with sulfate, nitrate, or chloride anions (Figure 2a, S2 & S3). The similar CVs exhibited by the different alkali salts suggest essentially no anion role in the overall ion sorption under negative polarization. Interestingly, CVs obtained using $Mg^{2+}$ deliver currents less than half of those seen with alkali metals. Moreover, increasing the electrolyte concentration to 1 M $MgSO_4$ did not increase the observed currents (Figure S4). The distinct response between monovalent alkali and divalent alkaline earth metal ions confirms that the cation-dominant ion sorption process under negative polarization is size-dependent. Indeed, CVs in electrolytes containing larger cations such as ammonium (Figure S5) and tetraethylammonium (TEA) display progressively decreasing currents and confirm the size-dependent ion sorption behavior in $Ni_3BHT$. This observation, combined with the lack of porosity in $Ni_3BHT$, provides a strong case for an intercalation-based charge-storage mechanism. Additionally, an elemental map (Figure S6) of the negatively polarized $Ni_3BHT$ electrodes using high-angle annular dark-field scanning transmission electron microscopy (HAADF-STEM) and energy dispersive spectroscopy (EDS) confirms the presence of alkali cations throughout the bulk of the electrode material, providing support for ion intercalation into $Ni_3BHT$.

Specific capacitances calculated from CVs at a low scan rate of 0.5 mV $s^{-1}$ (Figure 2b) evidence high gravimetric and volumetric values of ~400 F $g^{-1}$ and ~700 F $cm^{-3}$ for the alkali metal electrolytes. These values are on par with the state-of-the-art values for any MOF,[36] highlighting again that permanent porosity is not required for high performance in ECs. With increasing scan rates, a gradual decrease and a spread of capacitance values is noted between the alkali electrolytes, suggesting possible influence from factors such as varied ion sizes, solvation energies and ionic conductivities of the alkali salts (Figure 2b). Among the tested electrolytes, $K_2SO_4$ delivers the best power capability with high discharge capacitances of 260 and 177 F $g^{-1}$ at scan rates of 10 and 30 mV $s^{-1}$, corresponding to rapid discharge times of 60 and 20 s, respectively. The observed capacitance and charge capacity values are in agreement with our earlier results on the intercalation of $Li^+$ ions into $Ni_3BHT$ in an organic electrolyte (Figure S7). Electrolytes containing divalent or larger cations in $MgCl_2$, $(NH_4)_2SO_4$, and TEACl deliver lower capacitances of 250, 310, and 75 F $g^{-1}$, respectively, at a scan rate of 0.5 mV $s^{-1}$. This dependence of capacitance on the nature of the ion can be attributed to variations in effective ion sizes, which are in turn strongly dependent on the ionic radii and hydration enthalpies. For instance, $Mg^{2+}$ has a small ionic radius of 0.65 Å but has a strong hydration enthalpy of 1921 kJ/mol, leading to a large effective ion size and gives lower capacitance than alkali ions. With these results, $Ni_3BHT$ adds to a select group of electrode materials (e.g. MXenes, $MoS_2$) that intercalate multiple cations and store charge in ECs.[14,17]

Anion sorption in $Ni_3BHT$ was investigated by analyzing CVs at positive potential bias between 0 to 0.4 V. Tests in various nitrite and nitrate-based electrolytes display rectangular CVs (Figure 2c) and indicate continued ion sorption throughout an applied potential window of 0.4 V vs. OCP (Figure S8). However, CVs obtained using a variety of anions such as tetrafluoroborate, perchlorate and chloride (Figure S9 & S10) display unstable currents with highly resistive behavior. These data, similar to the behavior seen with cations under negative potentials, indicate an anion-specific ion sorption response under a positive bias. Moreover, a closer look at the anions suggests that the planar shape of nitrate and nitrite makes them uniquely suited to intercalate into the 2D layers of $Ni_3BHT$, while other larger anions are not allowed. Indeed, an elemental map of positively polarized $Ni_3BHT$ in $NaNO_3$ electrolyte obtained using HAADF-STEM-EDS identifies N throughout the bulk of the electrode (Figure S11). Moreover, further tests in electrolytes containing planar carbonate and bicarbonate anions display rectangular CVs that are similar to nitrates/nitrites and support the hypothesis of a size or shape-based anion intercalation into $Ni_3BHT$ (Figure S12). Notwithstanding, further modelling is necessary to understand anion intercalation and the role of solvent in these processes.

Specific capacitances calculated from CVs (Figure 2d) at a low scan rate of 0.5 mV $s^{-1}$ reveal gravimetric and volumetric values of ~220 F $g^{-1}$ and ~400 F $cm^{-3}$, in nitrate and nitrite electrolytes, respectively. $NaNO_3$ delivered the best power capability with discharge capacitances of 150 and 117 F $g^{-1}$ at scan rates of 7 and 15 mV $s^{-1}$, corresponding to rapid discharge times of 58 and 26 s, respectively. Notably, these capacitance values are only approximately half of those seen under negative potentials, and even lower than the value observed for the similarly-sized ammonium cation, altogether suggesting a difference in charge storage mechanisms between negative and positive bias. Overall, the unique ability of $Ni_3BHT$ to intercalate both cations and anions is, to our knowledge, the first such example in ECs.[17]

**Charge storage mechanism:** With the evidence of intercalation-based ion sorption in $Ni_3BHT$ in hand, we probed the kinetics and nature of charge storage under different polarizations using voltammetry and impedance-based methods. A nitrate electrolyte, 0.5 M $NaNO_3$, and a potassium electrolyte, 0.5 M $K_2SO_4$, were chosen as the best performing electrolytes for tests under positive and negative polarizations, respectively. CVs obtained at various scan rates display quasi rectangular shapes in both of these (Figure 3a, d). Analyzing these using the power-law relation:

$$i(v) = av^b \quad \text{(Equation 1)}$$

where *i* is the measured current at a given potential, V, $v$ is the scan rate, and *a* and *b* are adjustable parameters (*b* = 0.5 corresponds to a diffusion-limited battery-type ion sorption mechanism, whereas *b* = 1 indicates a surface-controlled capacitive or pseudocapacitive process)[40,41] gives a *b* value of ~ 0.9 for $Ni_3BHT$ under both polarizations (Figure 3b).

When *b* falls between 0.5 and 1, the total current is mathematically treated as a summation of diffusion-limited ($k_1v^{1/2}$) and capacitive ($k_2v$) components according to Eq. 2:[42]

$$i(v) = k_1v^{1/2} + k_2v \quad \text{(Equation 2)}$$

However, recent work on modelling CVs find that Equation 2 is an oversimplification of experimental currents and is particularly erroneous at high scan rates.[43–45] One approach to address this issue is using multiple step chronoamperometry (MUSCA) to reconstruct CVs, minimize ohmic losses, and allow application of Equation 2.[46] Elaborate reconstruction of $Ni_3BHT$ CVs using MUSCA finds $k_2$ values of 0.93 and 0.88 under negative and positive potentials, respectively, indicating that both $K^+$ and $NO_3^-$ ions intercalate predominantly in a capacitive fashion (Figures S13 & S14). Furthermore, cycling at a high scan rate of 30 mV $s^{-1}$ (Figure 3e) demonstrates 80 and 98% capacitance retention after 8000 cycles in $K_2SO_4$ and $NaNO_3$, respectively, highlighting the potential for long-term stability of $Ni_3BHT$ towards rapid intercalation.

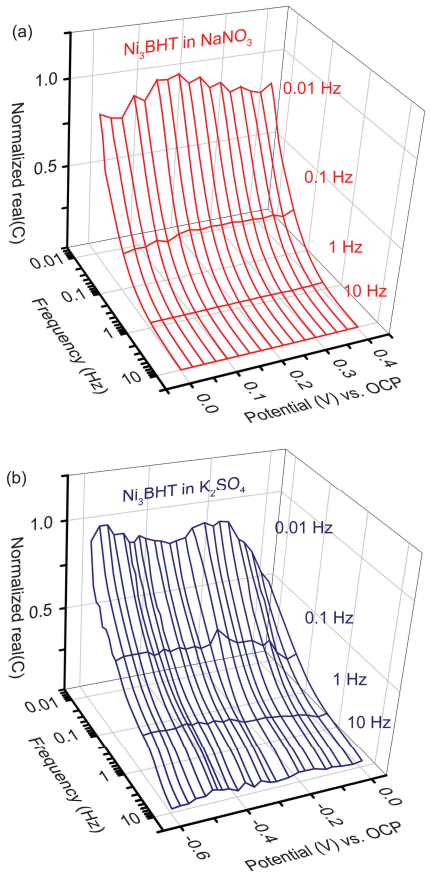


***Figure 4***. 3D plot representation of the normalized real (C) vs. frequency vs. potential for $Ni_3BHT$ in (a) 0.5 M $NaNO_3$ and (b) 0.5 M $K_2SO_4$ under positive and negative polarizations, respectively.

With the confirmation of rapid and stable intercalation in $Ni_3BHT$, we studied the nature of charge storage through impedance (Z) analysis at various applied potentials. A typical Nyquist representation of impedance responses from an EC consists of 3 frequency-dependent features; a semicircle, a 45° line Warburg region and a 90° capacitive branch at high, medium, and low frequencies, respectively. The semicircle appears as a result of contact resistance ($R_C$) at the current-collector/electrode interface with possible additional contributions from charge-transfer resistances ($R_{CT}$) within the electrode. Although $R_C$ is

10.1002/anie.202112811




potential-independent, charge-transfer events and the associated $R_{CT}$ vary with the applied potential. Similarly, the low-frequency imaginary im(Z) values, which directly correlate with the deliverable capacitance of an EC, are potential-independent in an EDLC but vary with applied potential when charge-transfer events are involved. Thus, the potential responses of $R_{CT}$ and im(Z) provide an excellent means to identify charge-transfer events in a given electrode.[19] Nyquist plots of $Ni_3BHT$ under variable positive potential (Figure 3c) display similar features with comparable high-frequency intercepts (~ 0.5 Ω $cm^2$), semicircle arcs (~2 Ω $cm^2$), and vertical capacitive branches in the low-frequency region. In comparison, spectra under increasingly negative potentials (Figure 3f) also show comparable high-frequency intercepts but display a gradual increase in the semicircle diameter (2-3 Ω $cm^2$) and a precipitous drop in im(Z) at low-frequencies. Interestingly, a calculation of diffusion resistances (σ) for cation intercalation in electrolytes containing different alkali ions found close values of 2.04, 1.94 and 1.45 $\Omega.s^{-1/2}.cm^2$ in $Li_2SO_4$, $Na_2SO_4$ and $K_2SO_4$ electrolytes, respectively (Figure S15). These low σ values in different electrolytes indicate rapid alkali ion transport in $Ni_3BHT$.

The observed impedance behaviors can be better represented using 3D Bode-style projections comprising calculated real(C) vs. frequency vs. potential plots.[47,48] Thus, the 3D Bode plot of $Ni_3BHT$ in $NaNO_3$ under positive potentials (Figure 4a) displays smooth curves with similar real(C) values across the applied potentials and frequencies. However, the data with $K_2SO_4$ under negative potentials (Figure 4a) show a more rugged pattern with potential-dependent variations in real(C). Expectedly, the traces corresponding to maximum real(C) values at the lowest frequency of 0.01 Hz mirror the CV responses seen in Figure 2a & 2c.

Overall, multiple key features of impedance remain invariant to applied positive potentials, thus identifying $NO_3^-$ intercalation into $Ni_3BHT$ as a purely capacitive process. To our knowledge, this qualifies as the first instance of a purely capacitive anion intercalation in ECs. On the other hand, the evolution of impedance features under negative potentials classifies cation intercalation in $Ni_3BHT$ as a charge-transfer induced behavior, described in some circles as intercalation pseudocapacitance (see above). It is worth reemphasizing here that the cation intercalation capacitance values in $Ni_3BHT$ (Figure 2b) are twice as large as the values observed for anion intercalation (Figure 3b), in agreement with the different charge storage mechanisms proposed above. Overall, these data identify $Ni_3BHT$ as a unique 2D material that intercalates ions both in capacitive and pseudocapacitive charge storage processes.

**Spectroscopic analysis.** Insight into the compositional and structural evolution of $Ni_3BHT$ under potential bias came from various X-ray techniques. For practical purposes, studies were done using $NaNO_3$ as a single electrolyte under both negative and positive polarization because both $Na^+$ and $NO_3^-$ ions intercalate efficiently within $Ni_3BHT$. A comparison of *ex-situ* X-ray photoelectron spectra (XPS) of pristine and polarized samples finds that the C 1s and Ni 2p peaks are unaffected by both positive and negative polarizations (Figure S16), and that the only observable changes occur with the S 2p peak (Figure 5). Specifically, a new peak appears at 161.2 eV in the negatively polarized sample. This peak diminishes and disappears upon reverting the sample to 0 V and beyond towards +0.4 V. This reversible behavior points to changes in composition under negative polarization. Deconvolution of the S 2p signal (Figure S17) identifies the feature at 161.2 eV as a $S^{\delta-}$-$Na^+$ ion-pair component that likely emerges from electrochemical reduction and subsequent intercalation of Na ions to partially electronegative S sites. This ligand-centered process has been noted in several previous studies of Ni-bis(dithiolene) complexes[49] and a recent study describing the behavior of related $Cu_3BHT$ in Li-ion batteries.[50] Overall, the XPS data confirm a pseudocapacitive charge storage mechanism for cation intercalation and a capacitive process for anion intercalation.

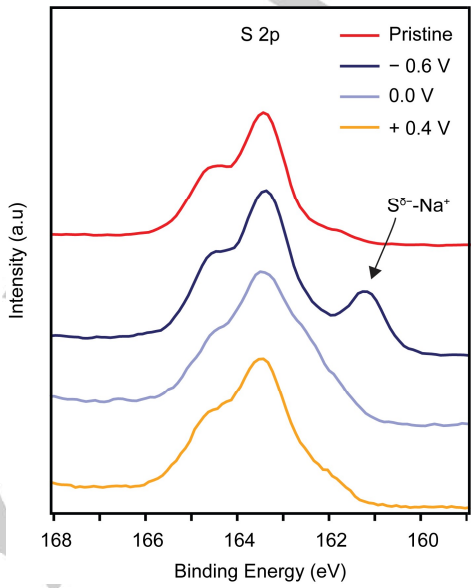


***Figure 5.*** High-resolution S 2p X-ray photoelectron spectra of $Ni_3BHT$ samples that are polarized under *ex-situ* conditions. A new S-$Na^+$ component reversibly appears under negative polarization.

Further insight into the structural evolution of $Ni_3BHT$ under polarization was gained from *ex-situ* and *in-situ* X-ray diffraction (XRD) analyses. Diffraction patterns from polarized samples display a minor shift in the (001) reflection from 25.8° to 25.2° (Figure S18), indicating lattice expansion during ion sorption. Further evidence for lattice expansion was provided by a cryogenic electron microscopy method called microcrystal electron diffraction (ED), which displayed a shift in the (001) peak of a positively polarized sample (Figure S19). These small, albeit noticeable changes in lattice parameters provide strong support for an intercalation-based charge-storage mechanism in $Ni_3BHT$. Interestingly, *in-situ* wide-angle X-ray scattering (WAXS) patterns of pristine and polarized samples remained largely similar (Figure S20), highlighting that the observed changes in X-ray and electron diffraction patterns are minor.

**Discussion:** The dual-ion intercalation in $Ni_3BHT$ allows an examination of the two leading hypotheses that explain origin of charge storage in intercalation-based EC electrodes. The prevalent concept of intercalation-pseudocapacitance treats intercalation as a redox-driven process, wherein the redox sites are localized and display a potential-dependent variance that can be identified in the spectroscopic features.[13] The alternative hypothesis treats intercalation-electrodes as electronic conductors that have conduction bands, instead of localized

redox states; any variations in the electrode composition during EC operation would then be delocalized and probably minimal.[24] In the case of $Ni_3BHT$, cation intercalation displays reversible appearance of an $S^{\delta-}$-$Na^+$ component in XPS, suggesting a localized redox behavior and synergy with the popular concept of pseudocapacitance. However, anion intercalation in $Ni_3BHT$ diverges from the conventional notion of redox-driven intercalation, and aligns with the concept of capacitance driven by greater electrolyte access to interlayer surfaces of electronic conductors.

The observed dual-ion intercalation in $Ni_3BHT$ raises interesting questions about factors behind such a behavior and how this material compares with other 2D MOFs and CPs. Reports on related $Ni_3HITP_2$ and NiHIB have previously ascribed ion sorption as ion insertion in the pores or as a surface-based redox activity with no hint of intercalation between the 2D layers. A structural comparison between $Ni_3BHT$, $Ni_3HITP_2$, and NiHIB evidences inter-layer spacings of 3.45, 3.30 and 3.19 Å, respectively. It is reasonable to attribute the larger inter-layer spacing and weaker inter-layer interactions in $Ni_3BHT$ to promote intercalation. Nevertheless, renewed focus on studying intercalation in other 2D MOFs and CPs through ion size-based analyses is essential to identify intercalation candidates and formulate broader design principles. Overall, $Ni_3BHT$ exhibits unique electrochemical features and provides an excellent platform to test and further our understanding of intercalation processes in ECs.

## Conclusion

$Ni_3BHT$ is a representative example for non-porous coordination polymers that demonstrates reversible charge storage through ion intercalation. Multiple electrolytic ions including $Li^+$, $Na^+$, $K^+$, $NH_4^+$, $NO_3^-$ and $NO_2^-$ were found to readily intercalate under external polarization. High gravimetric and volumetric specific capacitances of 413 F $g^{-1}$ and 720 F $cm^{-3}$ were observed despite the absence of canonical porosity in $Ni_3BHT$. Extensive electrochemical characterization revealed that cation intercalation in $Ni_3BHT$ can be interpreted as pseudocapacitive, whereas anion intercalation is clearly purely capacitive. This dual-ion intercalation and unique charge storage mechanisms are discussed and compared within the purview of current leading hypotheses for intercalation-based electrodes. Overall, this work opens up 2D CPs as a class of diverse and tunable materials that merit further study in the context of ECs.

## Acknowledgements

This work was supported by Automobili Lamborghini S.P.A. This research used resources of the Center for Functional Nanomaterials and the SMI beamline (12-ID) of the National Synchrotron Light Source II, both supported by the U.S. DOE Office of Science Facilities at Brookhaven National Laboratory under Contract No. DE-SC0012704. Part of this work (XPS, HAADF-STEM and EDS) used the MRSEC Shared Experimental Facilities at MIT, supported by the National Science Foundation under Award No. DMR-1419807. We thank Dr. Yong Zhang for his assistance with HAADF-STEM and EDS measurements. Specimens for Cryo-EM were prepared and imaged at the Automated Cryogenic Electron Microscopy Facility at MIT.nano on a Talos Arctica microscope, which was a gift from the Arnold and Mabel Beckman Foundation.

**Keywords:** Intercalation • Pseudocapacitance • Coordination polymers • Electrochemical Capacitors

[1] P. Simon, Y. Gogotsi, *Nat. Mater.* **2008**, *7*, 845–854.
[2] P. Simon, Y. Gogotsi, *Nat. Mater.* **2020**, *19*, 1151–1163.
[3] F. Béguin, V. Presser, A. Balducci, E. Frackowiak, *Adv. Mater.* **2014**, *26*, 2219–2251.
[4] M. Salanne, B. Rotenberg, K. Naoi, K. Kaneko, P.-L. Taberna, C. P. Grey, B. Dunn, P. Simon, *Nat. Energy* **2016**, *1*, 1–10.
[5] T. Brousse, D. Bélanger, J. W. Long, *J. Electrochem. Soc.* **2015**, *162*, A5185–A5189.
[6] X. Wu, Y. Qi, J. J. Hong, Z. Li, A. S. Hernandez, X. Ji, *Angew. Chem. Int. Ed.* **2017**, *56*, 13026–13030.
[7] G. Liang, F. Mo, X. Ji, C. Zhi, *Nat. Rev. Mater.* **2021**, *6*, 109–123.
[8] B. E. Conway, *J. Electrochem. Soc.* **1991**, *138*, 1539–1548.
[9] V. Augustyn, J. Come, M. A. Lowe, J. W. Kim, P.-L. Taberna, S. H. Tolbert, H. D. Abruña, P. Simon, B. Dunn, *Nat. Mater.* **2013**, *12*, 518–522.
[10] V. Augustyn, P. Simon, B. Dunn, *Energy Environ. Sci.* **2014**, *7*, 1597–1614.
[11] T. Brezesinski, J. Wang, S. H. Tolbert, B. Dunn, *Nat. Mater.* **2010**, *9*, 146–151.
[12] M. R. Lukatskaya, O. Mashtalir, C. E. Ren, Y. Dall'Agnese, P. Rozier, P. L. Taberna, M. Naguib, P. Simon, M. W. Barsoum, Y. Gogotsi, *Science* **2013**, *341*, 1502–1505.
[13] S. Fleischmann, J. B. Mitchell, R. Wang, C. Zhan, D. Jiang, V. Presser, V. Augustyn, *Chem. Rev.* **2020**, *120*, 6738–6782.
[14] C. Choi, D. S. Ashby, D. M. Butts, R. H. DeBlock, Q. Wei, J. Lau, B. Dunn, *Nat. Rev. Mater.* **2020**, *5*, 5–19.
[15] M. Ghidiu, M. R. Lukatskaya, M.-Q. Zhao, Y. Gogotsi, M. W. Barsoum, *Nature* **2014**, *516*, 78–81.
[16] M. Acerce, D. Voiry, M. Chhowalla, *Nat. Nanotechnol.* **2015**, *10*, 313–318.
[17] Y. Liu, S. P. Jiang, Z. Shao, *Mater. Today Adv.* **2020**, *7*, 100072.
[18] J. T. Mefford, W. G. Hardin, S. Dai, K. P. Johnston, K. J. Stevenson, *Nat. Mater.* **2014**, *13*, 726–732.
[19] T. S. Mathis, N. Kurra, X. Wang, D. Pinto, P. Simon, Y. Gogotsi, *Adv. Energy Mater.* **2019**, *9*, 1902007.
[20] P. Simon, Y. Gogotsi, B. Dunn, *Science* **2014**, *343*, 1210–1211.
[21] Z. Chen, V. Augustyn, J. Wen, Y. Zhang, M. Shen, B. Dunn, Y. Lu, *Adv. Mater.* **2011**, *23*, 791–795.
[22] J. W. Kim, V. Augustyn, B. Dunn, *Adv. Energy Mater.* **2012**, *2*, 141–148.
[23] X. Wang, T. S. Mathis, K. Li, Z. Lin, L. Vlcek, T. Torita, N. C. Osti, C. Hatter, P. Urbankowski, A. Sarycheva, M. Tyagi, E. Mamontov, P. Simon, Y. Gogotsi, *Nat. Energy* **2019**, *4*, 241–248.
[24] C. Costentin, J.-M. Savéant, *Chem. Sci.* **2019**, *10*, 5656–5666.
[25] C. Costentin, T. R. Porter, J.-M. Savéant, *ACS Appl. Mater. Interfaces* **2017**, *9*, 8649–8658.
[26] M. Hmadeh, Z. Lu, Z. Liu, F. Gándara, H. Furukawa, S. Wan, V. Augustyn, R. Chang, L. Liao, F. Zhou, E. Perre, V. Ozolins, K. Suenaga, X. Duan, B. Dunn, Y. Yamamto, O. Terasaki, O. M. Yaghi, *Chem. Mater.* **2012**, *24*, 3511–3513.
[27] J.-H. Dou, L. Sun, Y. Ge, W. Li, C. H. Hendon, J. Li, S. Gul, J. Yano, E. A. Stach, M. Dincă, *J. Am. Chem. Soc.* **2017**, *139*, 13608–13611.
[28] A. C. Hinckley, J. Park, J. Gomes, E. Carlson, Z. Bao, *J. Am. Chem. Soc.* **2020**, *142*, 11123–11130.
[29] M. Yu, R. Dong, X. Feng, *J. Am. Chem. Soc.* **2020**, *142*, 12903–12915.
[30] T. Kambe, R. Sakamoto, K. Hoshiko, K. Takada, M. Miyachi, J.-H. Ryu, S. Sasaki, J. Kim, K. Nakazato, M. Takata, H. Nishihara, *J. Am. Chem. Soc.* **2013**, *135*, 2462–2465.
[31] X. Huang, P. Sheng, Z. Tu, F. Zhang, J. Wang, H. Geng, Y. Zou, C. Di, Y. Yi, Y. Sun, W. Xu, D. Zhu, *Nat. Commun.* **2015**, *6*, 1–8.
[32] L. S. Xie, G. Skorupskii, M. Dincă, *Chem. Rev.* **2020**, *120*, 8536–8580.
[33] J.-H. Dou, M. Q. Arguilla, Y. Luo, J. Li, W. Zhang, L. Sun, J. L. Mancuso, L. Yang, T. Chen, L. R. Parent, G. Skorupskii, N. J. Libretto, C. Sun, M. C. Yang, P. V. Dip, E. J. Brignole, J. T. Miller, J. Kong, C. H. Hendon, J. Sun, M. Dincă, *Nat. Mater.* **2021**, *20*, 222–228.
[34] S. Bi, H. Banda, M. Chen, L. Niu, M. Chen, T. Wu, J. Wang, R. Wang, J. Feng, T. Chen, M. Dincă, A. A. Kornyshev, G. Feng, *Nat. Mater.* **2020**, *19*, 552–558.
[35] D. Sheberla, J. C. Bachman, J. S. Elias, C.-J. Sun, Y. Shao-Horn, M. Dincă, *Nat. Mater.* **2017**, *16*, 220–224.
[36] D. Feng, T. Lei, M. R. Lukatskaya, J. Park, Z. Huang, M. Lee, L. Shaw, S. Chen, A. A. Yakovenko, A. Kulkarni, J. Xiao, K. Fredrickson, J. B. Tok, X. Zou, Y. Cui, Z. Bao, *Nat. Energy* **2018**, *3*, 30–36.

10.1002/anie.202112811





[37] M. R. Lukatskaya, D. Feng, S.-M. Bak, J. W. F. To, X.-Q. Yang, Y. Cui, J. I. Feldblyum, Z. Bao, *ACS Nano* **2020**, *14*, 15919–15925.
[38] A. Schneemann, R. Dong, F. Schwotzer, H. Zhong, I. Senkovska, X. Feng, S. Kaskel, *Chem. Sci.* **2021**, *12*, 1600–1619.
[39] H. Banda, J.-H. Dou, T. Chen, N. J. Libretto, M. Chaudhary, G. M. Bernard, J. T. Miller, V. K. Michaelis, M. Dincă, *J. Am. Chem. Soc.* **2021**, *143*, 2285–2292.
[40] T. Liu, W. G. Pell, B. E. Conway, *Electrochim. Acta* **1997**, *42*, 3541–3552.
[41] B. E. Conway, D. C. W. Kannangara, *J. Electrochem. Soc.* **1987**, *134*, 906–918.
[42] J. Wang, J. Polleux, J. Lim, B. Dunn, *J. Phys. Chem. C* **2007**, *111*, 14925–14931.
[43] C. Costentin, *J. Phys. Chem. Lett.* **2020**, *11*, 9846–9849.
[44] M. Forghani, S. W. Donne, *J. Electrochem. Soc.* **2019**, *166*, A1370–A1379.
[45] M. Forghani, S. W. Donne, *J. Electrochem. Soc.* **2018**, *165*, A664–A673.
[46] H. Shao, Z. Lin, K. Xu, P.-L. Taberna, P. Simon, *Energy Storage Mater.* **2019**, *18*, 456–461.
[47] P. L. Taberna, P. Simon, J. F. Fauvarque, *J. Electrochem. Soc.* **2003**, *150*, A292–A300.
[48] J. S. Ko, M. B. Sassin, D. R. Rolison, J. W. Long, *Electrochim. Acta* **2018**, *275*, 225–235.
[49] T. Kusamoto, H. Nishihara, *Coord. Chem. Rev.* **2019**, *380*, 419–439.
[50] Z. Wu, D. Adekoya, X. Huang, M. J. Kiefel, J. Xie, W. Xu, Q. Zhang, D. Zhu, S. Zhang, *ACS Nano* **2020**, *14*, 12016–12026.

10.1002/anie.202112811

WILEY-VCH

RESEARCH ARTICLE

**Entry for the Table of Contents**

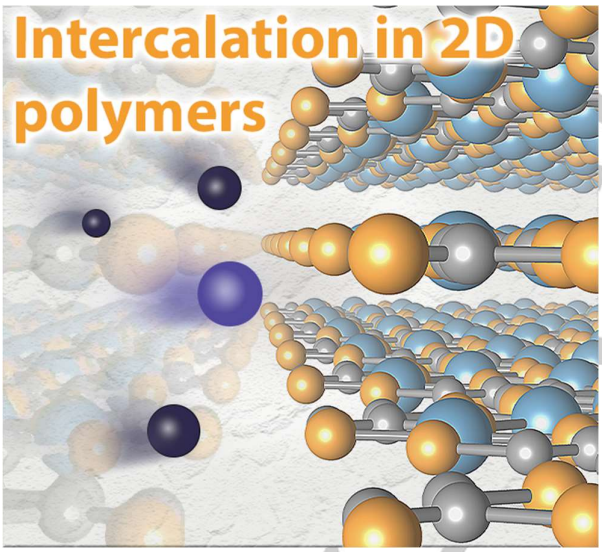


A two-dimensional coordination polymer ($Ni_3BHT$) demonstrates rapid and reversible intercalation of both cations and anions in an electrochemical capacitor (EC). This first observation of dual-ion intercalation in ECs presents a unique scenario, wherein cation intercalation in $Ni_3BHT$ is pseudocapacitive but anion intercalation is capacitive in nature.

Institute and/or researcher Twitter usernames: Mircea Dincă (@DincaGroupMIT), Harish Banda (@HarishBanda3), Jin-Hu Dou (@JinhuDou), Tianyang Chen (@TianyangChen7) and MIT Chemistry (@ChemistryMIT)